





Design of a Scaled Roller-rig Test Bench for Anti-slip Control Development for Railway Traction

Nihal Vishnu Vantagodi , Ahmed F. Abouzeid , *Member, IEEE*, Juan M. Guerrero , *Senior Member, IEEE*, Iban Vicente, Iker Muniategui, Aitor Endemaño, Fernando Briz , *Senior Member, IEEE*,

Abstract—Anti-slip control is a prominent part of modern railway traction control systems due both to performance and safety concerns. This paper explains the development of a scaled roller-rig test bench which emulates the rail and the wheel of a train. The final purpose of the developed roller-rig test bench is twofold: to study the theory/behaviour of existing anti-slip strategies and to test new designs, before their implementation in the real system. Estimation of adhesion coefficient using a disturbance observer method is explained and tested under various conditions. Anti-slip control is implemented in wheel drive using a direct method by adding a slip speed controller. The tests are conducted using both fixed roller speed and variable roller speed, i.e. dynamic roller. In this second case, train inertia emulation will be key. Two methods are proposed to emulate train inertia, being this the main contribution of this paper. Both methods are verified in simulation first, and further confirmed experimentally in the test bench.

Index Terms—Traction control, Anti-slip control, Roller-rig test bench, Train inertia emulation

I. INTRODUCTION

RAILWAY vehicles often require large tractive effort. Due to the design of wheel and rail, combined with the large elastic coefficient of steel, transfer of forces between the wheel and the rail occur through a small steel-to-steel contact area. While this is advantageous regarding frictional losses, it will curb the maximum force transfer. The maximum transferable force between the wheel and rail will not only be a function of design parameters such as wheel and rail shapes and materials, vehicle weight, etc. but also will be strongly affected by the surface conditions of rail [1]. Exceeding the maximum tractive force can produce an uncontrolled wheel slip, which can result in a number of unwanted effects, including reduced acceleration/deceleration performance [1], and also the risk of triggering torsional vibration phenomena [2]. This creates an interest and necessity to study slip phenomena and to develop anti-slip control methods.

Roller rigs are one of the important experimental setup that help in study and validation of the topics related to

Nihal Vishnu Vantagodi, Ahmed Fathy Abouzeid, Juan Manuel Guerrero and Fernando Briz are with the Department of Electrical, Electronic and Computer Engineering, University of Oviedo, Gijón, Spain (e-mail: vantagodinihal@uniovi.es; abouzeidahmed@uniovi.es; guerrero@uniovi.es; fbriz@uniovi.es). Ahmed Fathy Abouzeid is on leave with the Department of Electrical Engineering, Port-Said University, Egypt (e-mail: ahmed_abouzeid@eng.psu.edu.eg).

Iban Vicente, Iker Muniategui, Aitor Endemaño are with the Department of Traction systems, Ingeteam Power Technology, Zamudio, Spain (e-mail: iban.vicente@ingetteam.com; iker.muniategui@ingetteam.com; aitor.endemano@ingetteam.com).

This work was supported in part by the Government of the Principality of Asturias under Project AYUD/2021/50988.

railway vehicle dynamics [3], [4], including wheel-rail contact dynamics [5], braking system [6], slip control [7] and adhesion estimation [8], etc. Test rigs can be developed in full scale, where the dimensions of the wheel and forces are unchanged compared to the actual wheels [4]; and in scaled versions, where the wheel size and the related parameters are reduced in specific ratio [9].

In this paper, the design of a scaled roller-rig test bench intended to test anti-slip control methods is conducted. A key element for a realistic anti-slip control validation which has been ignored in literature is proper emulation of wheel/vehicle interactions, which requires train inertia emulation. The case of a train with infinite inertia will be considered first, as this significantly simplifies the control of the test bench. Then, emulation in the test bench of a finite train inertia will be considered. This will allow to reproduce the impact of anti-slip control on train speed. Two different approaches for inertia emulation are proposed in this paper: 1) using a disturbance observer; 2) using an adhesion torque observer. The proposed methods are first evaluated by means of simulation using MATLAB-Simulink. Further they are verified experimentally on the developed test rig.

The paper is structured as follows: Section II provides details about the real train system, adhesion-slip curve and the anti-slip control method being used. Section III explains the development of the roller-rig test bench. Section IV explains the anti-slip control method implemented in the wheel drive of the test bench, and the inertia emulation concept with the two proposed methods. Section V provides the experimental results obtained from the test bench on anti-slip control with inertia emulation. Section VI discusses the findings and conclusions.

II. SYSTEM DESCRIPTION

The general schematic representation of an electric locomotive traction drive is as shown in Fig. 1. The ac overhead line supplies the locomotive through the pantograph. The transformer steps down the voltage of the overhead line and feeds the four quadrant converter (4QC), which converts the ac into dc voltage. The dc link voltage is smoothed by the capacitor C_{dc} and is filtered by the (2F) filter [10]. The chopper is used for dc link over-voltage protection. Traction inverter controls the torque produced by the motors, different control strategies can be used for this purpose [11]. Motors are mechanically coupled with the gear then to the traction wheel. Advanced locomotives have the adhesion control along with the torque control. Slip control enables better performance

during slippery condition, and can also contribute to reduce the risk of torsional vibration in the wheel axle [12], [13].

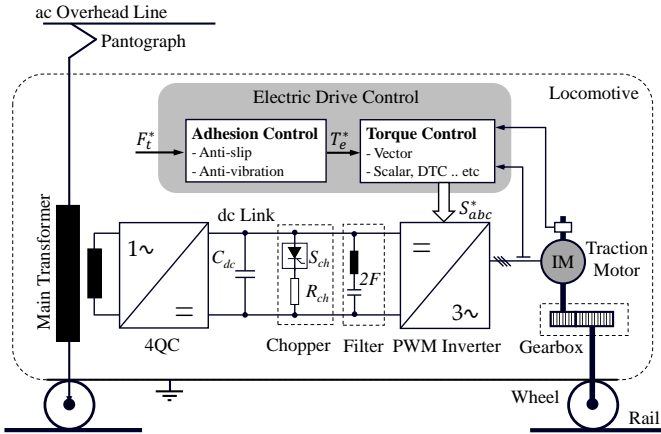


Fig. 1: Main elements of traction drive for real train.

Without the slippage, traction force F_t is equal to the tangential force and is given by (1), where T_m is motor torque after the gear, n is number of motors and r_w is traction wheel radius.

$$F_t = n \frac{T_m}{r_w} \quad (1)$$

The simplified force balance equation in the real train can be defined by (2), where m_t is train mass, B is the friction, v_t is train linear velocity and F_{lt} is the total load force.

$$F_t - F_{lt} = m_t \frac{dv_t}{dt} + B \cdot v_t \quad (2)$$

Total load forces given by (3) comprise of the aerodynamic force F_{lA} (4), the rolling friction force F_{lR} (5), and the gradient force F_{lG} (6), which are subtracted from the adhesive force to obtain the net force F_{net} (see Fig. 2). Similarly, the total load torque (T_{lt}) is subtracted from the adhesive torque (T_a) to obtain net torque, T_{net} .

$$F_{lt} = F_{lA} + F_{lR} + F_{lG} \quad (3)$$

$$F_{lA} = \frac{1}{2} C_d A_f \rho v_t^2 \quad (4)$$

$$F_{lR} = C_r m_t g \quad (5)$$

$$F_{lG} = m_t g \sin \theta \quad (6)$$

where C_d is drag coefficient, A_f is frontal area, ρ is air density, C_r is rolling friction coefficient, g is the acceleration of gravity and θ is gradient angle in degree. The total load torque T_{lt} can be obtained from the load force F_{lt} using the radius of the wheel as mentioned in Fig. 2.

Relationship between angular and linear velocities is given in (7) where ω_w is the angular velocity of the traction wheel.

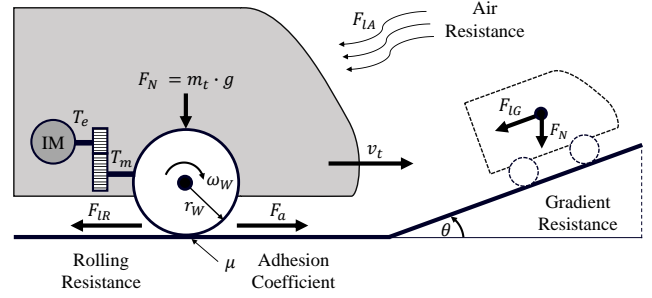


Fig. 2: Representation of train load forces and load torque.

$$v_t = \omega_w \cdot r_w \quad (7)$$

Adhesive force F_a is the force that can be transferred from the wheel onto the rail and is given by (8), where F_N is the normal force and μ is adhesion coefficient [14].

$$F_a = \mu \cdot F_N = \mu \cdot m_t \cdot g \quad (8)$$

The adhesion coefficient μ is a measure of the wheel-rail contact quality, which depends on the rail surface, environmental condition, temperature of the contact point, etc. The adhesion coefficient will be also significantly affected by the slip, which occurs when the angular velocity of the wheel doesn't match train linear velocity v_t (9).

$$\omega_w \cdot r_w \neq v_t \quad (9)$$

A. Adhesion-Slip Relation

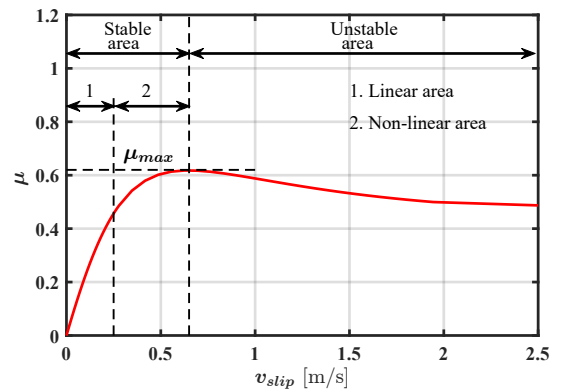


Fig. 3: Theoretical example adhesion-slip curve.

Variation of adhesion coefficient with respect to the slip velocity is called adhesion-slip curve in railway industry. An example plot is shown in Fig. 3. Based on the sign of the derivative of μ with respect to slip speed, the curve shown in Fig. 3 can be divided into two main regions. Positive values of $d\mu/dv_s$ correspond to the stable region. In this region, an increase of slip results in an increase of μ , and consequently of the tractive effort, eventually reducing slip. The stable region is

seen to consist of two sub-regions: 1) linear area, the adhesion coefficient increases almost linearly with the slip velocity; 2) nonlinear area, $d\mu/dv_s$ reduces progressively, eventually reaching the maximum adhesion coefficient when $d\mu/dv_s = 0$.

If the slip surpasses this maximum, then $d\mu/dv_s < 0$, which corresponds to the unstable region. In this region, an increase of slip speed will result in a reduction of adhesive force. When this occurs, wheel speed is no longer linked to train speed. Equation (10) holds in this case, where J_a accounts for axle inertia.

$$T_m - F_a r_w = J_a \frac{d\omega_w}{dt} \quad (10)$$

It is observed from (10) that if traction motor torque T_m remains invariant, a decrease of F_a will result in a sustained increase of ω_w . Since F_a is decreasing, tractive force F_t , and consequently train speed will decrease too, slip speed consequently increasing steadily.

B. Anti-Slip Control

Slip control methods are aimed to maintain the slip velocity of the vehicle within the linear region and not far from the maximum adhesion coefficient value, in order to achieve the maximum possible traction effort [15]. An overview of the available slip control methods is provided in [16]. The method used in this paper being a direct type, a speed controller is used to follow the commanded slip during slippage.

The anti-slip control is implemented based on 'slip velocity control to a constant value method' [16], the control schematic is shown in Fig. 4. The torque command T_{mW}^* is provided as a ramp signal to emulate the increase in velocity of the train avoiding jerk and considering the comfort and safety of passengers. The torque reference T_{mW}^{ref} is applied to the torque controller. Fast and precise torque control is needed to avoid excessive slippage. Rotor field-oriented control (RFOC) was selected and will be used in developed the test rig as well. Voltage commands produced by RFOC are modulated using PWM to generate the pulses $S_{abc,W}^*$ controlling inverter switches. Other control methods could be used, e.g. scalar, DTC, etc. [11], but noting that a degradation of either dynamic response of the control, or accuracy of torque estimation, will affect to the accuracy of the wheel/roller contact emulation.

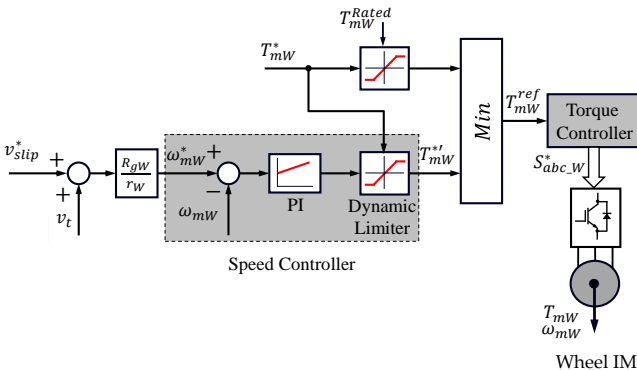


Fig. 4: Wheel drive with slip control.

When the torque commanded exceeds the adhesion limit, slip occurs in the wheels. When the slip occurs, the controller maintains the slip at the reference value v_{slip}^* such that it maintains the adhesion value at maximum and in the stable region. The required slip is achieved by the speed controller. The wheel speed command ω_{mW}^* is calculated from the slip velocity reference and the train velocity v_t using the gear ratio R_{gW} and the wheel radius r_w . The controller receives this speed command and provides the torque reference. The output of controller is saturated and this can be achieved using two methods, the static and dynamic saturation which are explained in Section IV-B. Dynamic limiter is used because of better performance compared to static limiter and the saturated output, T_{mW}^* is fed to the block which selects the minimum of the two torque values. Under operation without slip, torque from the ramp command will be fed to the torque controller block and during slippage, the torque command from speed controller will be less compared to the ramp command and hence will be provided to the torque controller block. Anti-slip control implementation in the test bench is addressed in Section IV.

III. SCALED ROLLER-RIG DESIGN

Either full scale or scaled roller rig test bench can be used to perform the tests needed to validate control strategies before introducing them in the real train. In the test bench, the actual rail is normally replaced by a wheel, which hereafter will be denoted as the roller. Use of scaled designs have obvious advantages in terms of cost and manageability. However, special care is required to ensure that key properties of the real system remain in the scaled version. This section explains the scaling and development of the test bench.

Depending on the purpose of the development of the test rig, to reduce the effect of scaling the dimensions, a suitable scientific approach must be taken while performing scaling. The scaling factors are derived based on the relation between physical quantities, the laws abiding them and the length scaling factor.

The ratio of full scale length l_f to the scaled model length l_s is the beginning step for setting the similarity of railway vehicles which is given by (11)

$$\delta_l = \frac{l_f}{l_s} \quad (\text{length}) \quad (11)$$

Density scaling factor is defined as (12), and using this the inertial quantities' scaling factors are defined as (13)

$$\delta_\rho = \frac{\rho_l}{\rho_s} \quad (\text{density}) \quad (12)$$

$$\delta_m = \frac{m_f}{m_s} = \delta_\rho \delta_l^3 \quad (\text{mass}) \quad (13)$$

These scaling factors form the basis of the scaling strategies. The three scaling methods which are often used in the roller rig development are MMU (Manchester Metropolitan University) method, DLR (Deutsches Zentrum für Luft- und Raumfahrt) method and INRETS (National Institute of Research on Transportation and Security) method [17]. Table I shows the

parameters considered for scaling and the comparison of the scaled values in SI units using the three techniques mentioned above. As the study purpose relates to vehicle dynamics of rail, MMU similitude method is chosen.

TABLE I: Comparison of roller-rig scaling techniques [17].

Scaling Variables		Scaling Method		
		MMU	DLR	INRETS
Geometry	Length	5	5	4
	Cross Section	25	25	16
Material	Density	1	0.5	1
	Mass	125	62.5	64
	Inertia	3125	1562.5	1024
System Variables	Time	1	$\sqrt{5}$	4
	Frequency	1	$1/\sqrt{5}$	$1/4$
	Velocity	5	$\sqrt{5}$	1
	Acceleration	5	1	4
	Angular velocity	1	$1/\sqrt{5}$	$1/4$

The roller-rig test bench is developed to simulate the conditions of a locomotive of 86 t with a nominal velocity of 10.56 m/s with 8 traction wheels, further details are given in Table II. The test bench is designed to have a single wheel and mass of the locomotive is considered to be equally distributed amongst the wheels. The scaled force F_{TR} acting on each wheel is given by (14)

$$F_{TR} = \frac{m_{loco} \cdot g}{n_{TR} \cdot \delta_m} \approx 0.843\text{kN} \quad (14)$$

where n_{TR} is number of traction wheels of real train and δ_m is mass scaling factor in MMU method with a value of 125 mentioned in Table I.

The scaled nominal linear speed of the wheel is given by (15)

$$v_{nom_{TR}} = \frac{v_{nom}}{\delta_v} = 2.11\text{m/s} \quad (15)$$

where δ_v is the velocity scaling factor in MMU method with a value of 5 mentioned in Table I.

The scaled wheel radius is 0.125 m. The roller radius was chosen to have twice the radius of wheel. Using the radius value and the scaled value of force and velocity (mentioned in Table II), the torque ($T = r \cdot F$) and angular speed ($\omega = v/r$) of the roller and wheel are calculated. Table II shows the parameters considered for scaling and the value obtained after the scaling using the MMU method.

IV. IMPLEMENTATION AND SIMULATION OF ANTI-SLIP CONTROL INCLUDING TRAIN INERTIA EMULATION

Validation of the test rig design and proposed emulation strategies is accomplished by means of simulation. First, the adhesion coefficient of the contact point of the roller-rig test bench has been estimated; this is discussed in section IV-A. The anti-slip control method explained in Section II-B is implemented in the wheel drive of the test bench. The schematic configuration of the test bench is shown in Fig.5(a). The physical system of wheel and rail is modelled using the contact point block as shown in 5(b). Wheel and roller angular speeds are obtained from the applied torques and the corresponding inertia. Angular speeds are converted to linear velocities v_W and v_R , in wheel and roller reference

TABLE II: Actual and Scaled parameters of roller-rig.

Parameter	Actual Value	Scaling Factor	Scaled Value	Unit
Wheel diameter	1.25	5	0.25	m
Roller diameter	infinite	-	0.50	m
Locomotive mass	86	125	0.688	t
Cargo mass	448.8	125	3.59	t
Force per wheel	105.4	125	0.84	kN
Velocity	10.56	5	2.11	m/s
Contact area	82-96 [18], [19]	25	3.28-3.84	mm ²
Inertia (Roll) x-axis per wheel	26113	781.2 ⁽¹⁾	33.42	kg m ²
Wheel Torque	5000	47.48 ⁽²⁾	105.3	Nm
Wheel Speed	3210	19.90 ⁽²⁾	161.3	r/min
Wheel Power	1084	608.9 ⁽²⁾	1.78	kW

⁽¹⁾ Inertia is calculated using $J = mr^2$. For train inertia, m is mass of locomotive and cargo per wheel and r is referred to wheel radius. For scaled inertia, m is scaled mass of locomotive and cargo per wheel and r is referred to test bench roller radius.

⁽²⁾ Derived from scaling factors and actual train and test bench gear ratios.

frame, from which the slip velocity v_{slip} is obtained. The adhesion-slip curve was obtained during a commissioning process and stored in a look-up table allowing a precise wheel-roller contact point modeling. This will be discussed later in section V-B. The look-up table is used further to obtain the adhesive force from the measured slip speed and the known normal force. Then using the gear ratio and radius of wheel and roller, the load torque for both motors are calculated.

First, a train with an infinite inertia is considered in Section IV-B. In this case, changes in the tractive effort will have no effects on train speed. This allows decoupled wheel and roller controls, significantly simplifying the implementation, but at the price of ignoring the dynamics of the train. The approach in Sections IV-D and IV-C considers a train with a finite inertia. Changes in the tractive force will affect in this case to train (roller) speed.

A. Adhesion Estimation Using Disturbance Observer

From Fig. 5, traction motor mechanical equation is given by (16)

$$T_{mW} = J_{mW} \frac{d\omega_{mW}}{dt} + B_{mW} \omega_{mW} + T_{lmW} \quad (16)$$

where T_{mW} and T_{lmW} are the electromagnetic torque and load torque seen by the motor respectively, J_{mW} is the combined wheel motor and inertia in motor reference, ω_{mW} is the motor speed and B_{mW} is viscous friction.

The adhesive force is calculated from the estimated load torque seen by the wheel \hat{T}_{lW} and wheel radius r_W as (17), R_{gW} being the motor-to-wheel gear. Terms with a hat ($\hat{\cdot}$) symbol stand for estimates of the corresponding variable or parameter.

$$\hat{F}_a = \frac{\hat{T}_{lW}}{r_W} = \frac{R_{gW} \hat{T}_{lmW}}{r_W} \quad (17)$$

For the motor, the load torque is the disturbance. A disturbance observer is then used to obtain the adhesion coefficient $\hat{\mu}$

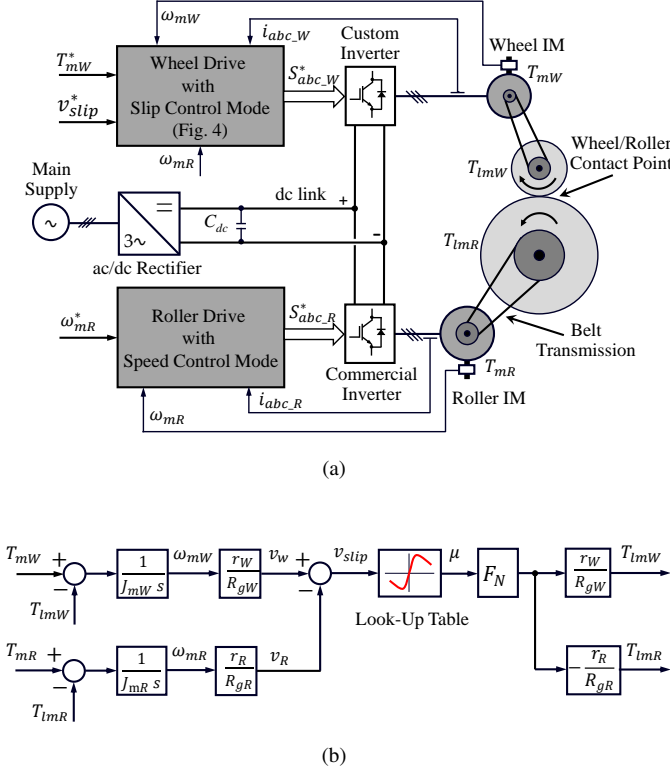


Fig. 5: Block diagram of roller-rig test bench. (a) Schematic representation of the overall control system; (b) Contact point model used in simulation. Look-up table is obtained experimentally as described in subsection V-B

[20]. Rearranging (16) for load torque and writing in Laplace domain, (18) is obtained.

$$T_{lmW}(s) = T_{mW}(s) - (J_{mW}s + B_{mW}) \cdot \omega_{mW}(s) \quad (18)$$

To avoid the pure derivative term in the numerator a low pass filter is used as proposed in [20], the estimated load torque \hat{T}_{lmW} being obtained as (19).

$$\hat{T}_{lmW}(s) = \hat{T}_{mW}(s) - (\hat{B}_{mW} + \frac{\hat{J}_{mW}}{\tau} - \frac{\hat{J}_{mW}/\tau}{\tau s + 1}) \cdot \omega_{mW}(s) \quad (19)$$

Finally, combining (8) and (17), the adhesion coefficient can be estimated from the estimated motor load torque as (20).

$$\hat{\mu} = R_{gW} \frac{\hat{T}_{lmW}}{F_N \cdot r_W} \quad (20)$$

B. Anti-Slip Control with Infinite Train Inertia

In this approach, changes on tractive force will have no effect on train speed. This might correspond to a scenario in which the gradient of railway progressively increases while the train is travelling at constant speed. This is shown schematically in Fig. 6. Tractive force increase following gradient force (6) increase might exceed the limit, causing slippage. Anti-slip control should keep the slip at the reference value in this case.

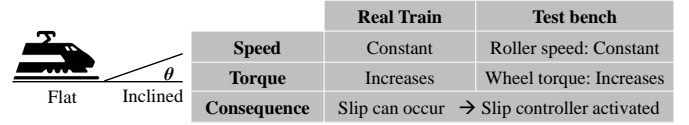


Fig. 6: Fixed roller speed scenario

In the described scenario, wheel is under torque control, torque command being a ramp. The roller is under speed control with the desired speed representing the train velocity. When the torque exceeds the limit, slip control is activated.

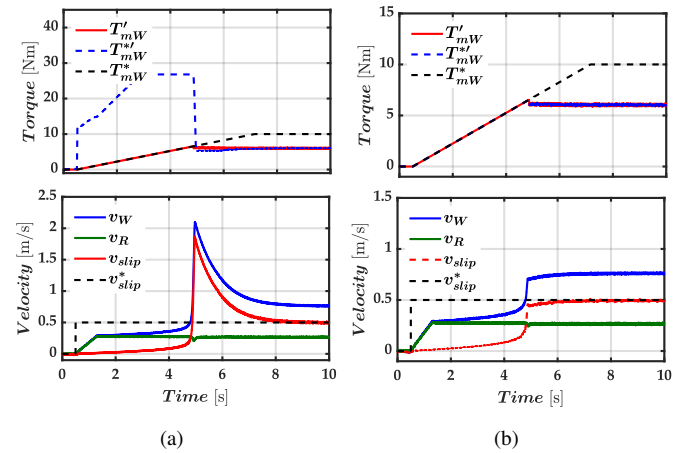


Fig. 7: Simulation results. Anti-slip control with fixed roller speed with static and dynamic saturation: (a) static limiter; (b) dynamic limiter. Top: Initial torque command T_{mW}^* ; output of slip control block $T_{mW}'^*$; torque command reaching the RFOC block of wheel drive $T_{mW}''^*$. Bottom: wheel and roller linear speeds, and slip speed

Special care must be taken in case saturation of the Proportional- Integral (PI) speed controller output in Fig. 4. Static saturation using rated torque as the limit is perhaps the most straightforward solution. Under normal operation, the actual slip velocity will be usually $\ll v_{slip}^*$. Thus the speed controller will saturate to rated torque in an attempt to achieve v_{slip}^* . When slip occurs, it takes time (≈ 2 s) for the slip PI controller to reduce the torque. During this time, an unacceptable overshoot of ($\approx 300\%$) in the slip velocity occurred, as seen in Fig. 7(a).

Hence to avoid this situation, a dynamic torque limiter is used which tracks the torque command and uses it as the torque limit for PI speed controller. When the ramp torque command cannot be transferred to the roller and the slip occurs, it shifts to the torque provided by the PI controller and limits the slip to the command value without having the overshoot. The results are shown in the Fig. 7(b), the improvement with respect to the static limiter case being readily observable.

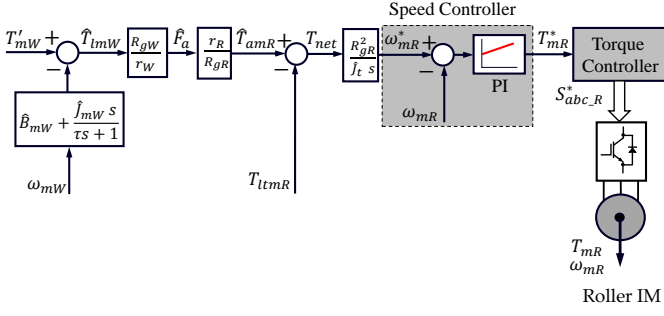


Fig. 8: Proposed inertia emulation using Disturbance Observer method.

C. Anti-slip Control with Proposed Train Inertia Emulation using Disturbance Observer

The tests in the previous method are performed with a fixed roller speed. As discussed, this would emulate a particular test condition wherein the gradient of the track increases but the velocity of the train remains constant. In a more general scenario, changes in the tractive force should produce changes in the train speed. To implement this, the speed of the roller, which represents the train linear speed, must change as a consequence of changes in wheel torque. It is noted that the inertia of the wheel in the test bench doesn't match the scaled train inertia. Wheel and roller inertia in motor reference frame are 0.002 kgm^2 and 0.007 kgm^2 respectively while the scaled train inertia in roller motor reference \hat{J}_{tmR} frame is 0.613 kgm^2 ($\hat{J}_{tmR} = \frac{\hat{J}_t}{R_{gR}^2}$, where $\hat{J}_t = 33.425 \text{ kgm}^2$ is scaled inertia calculated in Table II). I.e. the ratio between desired and actual roller inertia is ≈ 90 . Consequently, train inertia must be emulated by control.

The schematic of the inertia emulation using Disturbance Observer method is shown in Fig.8. The load torque of the wheel motor is estimated using the Disturbance Observer as in (19). The adhesive torque in roller motor reference at the wheel-rail contact, \hat{T}_{amR} , is estimated using the gear ratio and radius of wheel and roller. The net torque T_{net} is obtained after subtracting the total load torque (3). The roller speed command is obtained by integrating the net torque T_{net} and multiplying the inverse of equivalent train inertia in roller motor reference which is calculated dividing the scaled train inertia \hat{J}_t by the square of roller gear ratio (see Fig. 8). This serves as input for the roller speed controller, the following remarks can be made:

- This method is insensitive to roller inertia and friction while emulating the train inertia. It forces the roller to follow the required torque command to emulate the scaled inertia of the train.
- Wheel drive must share its torque command signal with the roller drive. This requires a fast and reliable communication channel between both drives. Delays and/or noise in the communications can result in significant degradation of the method.

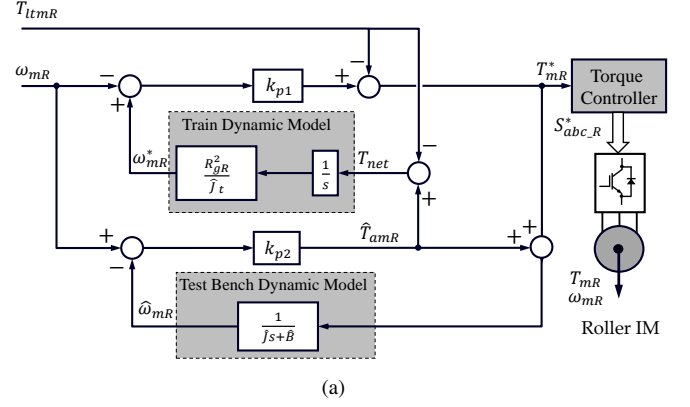


Fig. 9: Proposed inertia emulation using an adhesion torque observer (a) Adhesion Torque Observer model; (b) Contact point and roller drive dynamics.

D. Anti-slip Control with Proposed Train Inertia Emulation using Adhesion Torque Observer

The drawbacks of the previous method can be overcome by emulating train inertia independently in the roller drive without employing wheel signals considering the same test conditions. The block diagram of the method developed for emulating the train inertia using an Adhesion Torque Observer is shown in Fig. 9(a). It is derived from the concept proposed in [21] to emulate a wind turbine.

The torque that is transferred by the wheel onto the roller, adhesion torque T_a , depends on the wheel-roller contact point dynamics as shown in Fig. 9(b). T_a is estimated using a 'test bench dynamic model'. Then, using the estimated adhesion torque, a speed command for the roller, ω_{mR}^* , is obtained using a 'train dynamic model'. The test bench dynamic model accounts for the combined inertia \hat{J} and friction coefficients \hat{B} of the wheel, roller and the respective motors. The train dynamic model accounts for the scaled train inertia referred in roller motor reference frame.

Initially no torque is commanded to the roller. Due to T_a , the roller begins to rotate and gain speed, T_a -to- $-\omega_R$ relationship being determined by the overall (i.e. motor and roller) roller inertia J_R .

The adhesion torque in roller motor reference frame is estimated as \hat{T}_{amR} using the proportional gain k_{p2} given by (21) with the test bench dynamic model comprising of estimated roller and motor inertia.

$$\hat{T}_{amR} = k_{p2} \cdot (\omega_{mR} - \hat{\omega}_{mR}) \quad (21)$$

where the estimated roller speed $\hat{\omega}_{mR}$ is obtained by (22)

$$\hat{\omega}_{mR} = (\hat{T}_{amR} + T_{mR}^*) \cdot \frac{1}{(\hat{J}s + \hat{B})} \quad (22)$$

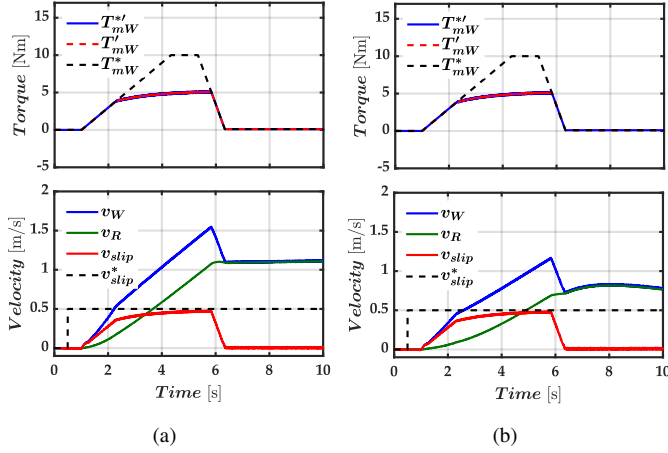


Fig. 10: Simulation results. Proposed inertia emulation methods (a) Disturbance Observer method; (b) Adhesion Torque Observer method. Top: Torque command T_{mW}^* ; output of slip control block T_{mW}^{*f} ; final output reaching the RFOC block of wheel drive T_{mW}^f . Bottom: wheel and roller linear speeds, and slip speed

The net torque is given by (23), where $T_{l_{tmR}}$ is total load torque in roller motor reference frame which correspond to the load force comprising of rolling friction, gradient and aerodynamic forces shown in Fig. 2.

$$T_{net} = \hat{T}_{amR} - T_{l_{tmR}} \quad (23)$$

The roller motor speed command ω_{mR}^* is calculated using train dynamic model which comprise of estimated scaled train inertia \hat{J}_t in roller motor reference frame and is given by (24).

$$\omega_{mR}^* = T_{net} \cdot \frac{R_{gR}^2}{\hat{J}_t} \cdot \frac{1}{s} \quad (24)$$

The proportional gain k_{p1} is used to calculate the torque that forces convergence of the estimated roller motor speed $\hat{\omega}_{mR}$ and the speed command ω_{mR}^* , the roller motor torque command is given by (25).

$$T_{mR}^* = k_{p1} \cdot (\omega_{mR}^* - \hat{\omega}_{mR}) \quad (25)$$

The gain k_{p1} is limited either by the roller drive torque control bandwidth or by the sampling frequency ω_s (26) as discussed in [21]

$$\frac{k_{p1}}{J_{mR}} < \frac{\omega_s}{2} \quad (26)$$

The gain k_{p2} is chosen to be (27) as mentioned in [21]

$$k_{p2} = \frac{2k_{p1}J_{mR}}{\hat{J}_{tmR}} \quad (27)$$

The results of the simulation of two methods analyzed for inertia emulation are presented in Fig. 10. Torque command T_{mW}^* follows a ramp up to the value required to achieve the target acceleration, and is later removed. It can be noticed that for the same train inertia, the increase in speed of roller v_R

TABLE III: Wheel and Roller test bench parameters.

System	Parameter	Wheel	Roller	Unit	Variable name
Wheel and Roller	Radius	0.125	0.25	m	r_W, r_R
	Force	843	843	N	-
	Torque	105.3	210.7	Nm	-
Transmission	Gear ratio	90/24	192/26	-	R_{gW}, R_{gR}
	Rating	4	5.5	kW	-
Traction Motor	Power used	1.78	1.78	kW	-
	Torque	28.1	28.5	Nm	T_{mW}, T_{mR}
	Speed	604.8	595.5	rpm	ω_{mW}, ω_{mR}
	Encoder Resolution	500	500	ppr	-
	Rating	4	15	kW	-
Motor-Wheel	Inertia ⁽¹⁾	0.002	0.007	kgm ²	J_{mW}, J_{mR}

⁽¹⁾ Inertia is calculated in wheel and roller motor reference frame respectively.

is lower ($\approx 27\%$) in the Adhesion Torque Observer method shown in Fig. 10(b) compared to the Disturbance Observer method of inertia emulation shown in bottom subplots of Fig. 10(a). On the other hand, developed torque is seen to be the same in both cases (see top subplots of Fig. 10(b) and 10(a)). This is expected as the Disturbance Observer method does not account for the roller friction and inertia, torque command being imposed only emulates train inertia. On the contrary, Adhesion Torque Observer method estimates adhesive torque from the roller speed, which accounts for test bench friction and inertia and hence has a lower speed. In both cases the slip velocity v_{slip} is achieved the reference value v_{slip}^* .

It is noted that the adhesion estimation methods presented in this section are intended for test bench operation and might not be suitable for adhesion estimation in actual locomotives.

V. EXPERIMENTAL VALIDATION

Experimental verification of the methods discussed in section IV is addressed in this section. Roller-rig is described in subsection V-A. Adhesion-slip curves are obtained in subsection V-B. These curves were used for contact point modeling (see Fig. 5(b)) and simulation analysis and verification discussed in subsection IV-A. Finally, validation of anti-slip control using the proposed inertia emulation methods discussed in subsections IV-B–IV-D is addressed in subsections V-C–V-E respectively.

A. Hardware Setup

Test bench parameters are given in Table III. Main elements of the test bench are discussed as following:

1) *Wheel and Roller*: The test bench has a wheel which emulates the traction wheel of the railway locomotive and a roller, which is a wheel with larger diameter, which emulates the rail. The manufacturing limit for roller diameter is 0.5 m and test rigs maintain a ratio of two or more between roller and wheel diameters. Hence, a diameter of 0.25 m was chosen for the wheel and 0.5 m for the roller (see Fig. 5(a) and Fig. 11(a)). The roller is a cylinder, i.e. its surface is flat. The

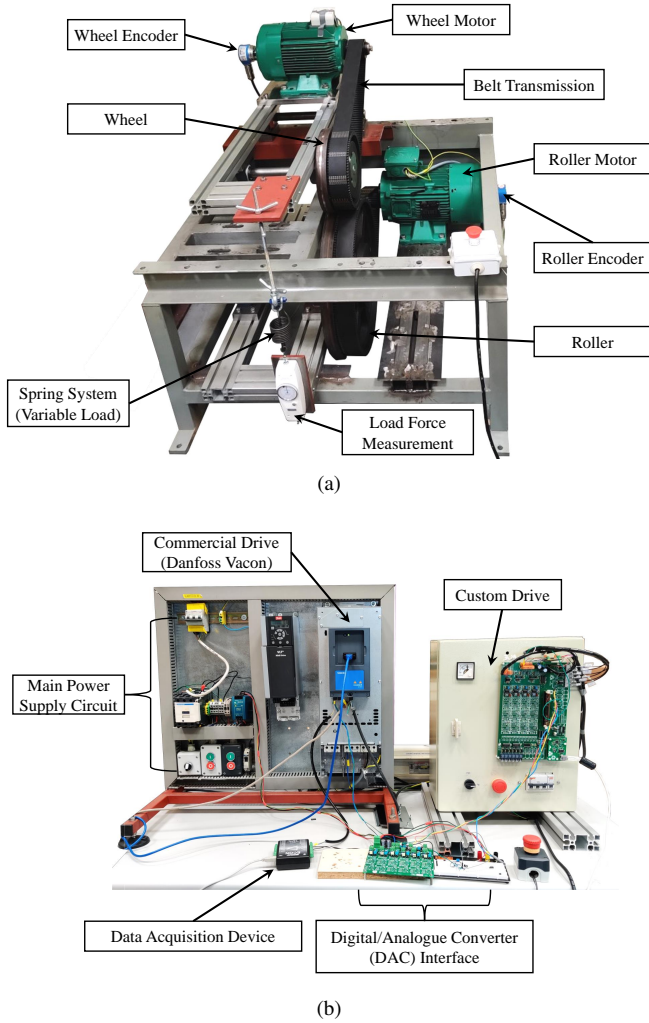


Fig. 11: Experimental setup: (a) Front view of roller rig test bench; (b) Electric Drives.

surface of the wheel is provided with a circular profile with radius 0.25 m, the resulting contact area is 3.93 mm^2 close to the required scaled value shown in Table II.

2) *Traction and Transmission Systems*: The traction system consists of the motors and the electric drives. Four-pole induction machines of 4 kW and 5.5 kW respectively are used for wheel and roller. From the wheel parameters calculated in Table II, it can be noticed that the required power and speed of wheel/roller are small but the required torque is large when compared to the induction motors rated value. Using a transmission between the wheel/roller and the motor allows achieving the required torque and speed. The gear ratios of the corresponding belt transmissions were selected to match rated torque-speed of the motors to wheel and roller requirements. The details can be found in Table III. The transmission between the motors, roller and wheel can either be gear drive, belt drive or chain drive.

Owing to the non-availability and time requirement to procure the gear drive of specific ratio to match the requirement, a V-belt drive is chosen. A commercial *Vacon NXP00385 Danfoss* drive is used to control the roller motor and a custom drive

is developed to control the wheel motor (see Fig. 11(b)). Both drives use rotor field-oriented control (RFOC) as mentioned in Section II-B. The Control Board of the custom drive contains the Digital Signal Controller (DSC) TMS320F28335 real time micro-controller from Texas Instruments which controls the operation of the drive with 10 kHz for both sampling and switching frequencies [22]. Additionally, the control board contains the input/output interface circuits for current, speed measurements and Pulse-Width Modulated (PWM) signals transmission for the power module.

Torque and speed of roller and wheel motors are needed for slip and torque control. Torques are estimated from RFOC variables, i.e. stator measured currents and estimated rotor flux [11]; speeds are obtained from 500 ppr encoders attached at wheel and roller motors.

3) *Wheel Load Adjustment*: The force applied by the wheel on the roller can be varied by the spring system, it is measured using a force gauge. The normal force can be varied between 380 N, which occurs when the spring is not stretched and all the force is due to wheel system mass, and 1380 N (see Fig. 11(a)).

4) *Visualization and Data Analysis*: Roller and wheel speeds are obtained from encoders (500 ppr of resolution) attached at the corresponding motors. Torques are estimated from RFOC variables. All the relevant signals involved in wheel and roller control can be exported using Pulse-Width Modulated (PWM) signals from the drives, and captured by a multi-channel acquisition system for visualization and results analysis (see Fig. 11(b)). Results shown in Fig. 12 to Fig. 16 have been obtained using this method.

B. Adhesion-Slip Curves

To validate the proper operation of the test bench and the consistency of the results, multiple tests were conducted to obtain adhesion-slip curves between wheel and roller under different operating conditions. Both drives were operated in speed control for these tests. For each test, a base speed is fixed for the roller and then the wheel is commanded to sweep the desired slip range. The adhesion value is calculated using (20). Tests were performed varying the load applied using the spring system and the roller speed. It is observed from Fig. 12(a) that adhesion decreases as load increases. Fig. 12(b) shows that adhesion increases with increase in roller speed.

Moreover, additional tests are also conducted to obtain the adhesion curves in various conditions to have a real-world scenario. The results obtained are shown in Fig. 13. The results show that adhesion is maximum in dry conditions and reduces with water, soap water, and is least with grease. This is consistent with the results reported using the roller rig test bench in [3] and the results obtained using a real train in [23]. In this context, it is worth mentioning that the adhesion estimation accuracy is relying on the estimated wheel motor torque as seen in (19) and (20). The torque observer was calibrated and tested experimentally, the estimation error being $< 4\%$. Consequently, the steady-state error in the estimated adhesion coefficient is expected to be $< 4\%$. Transient errors will depend on the first-order low-pass filter (LPF) time

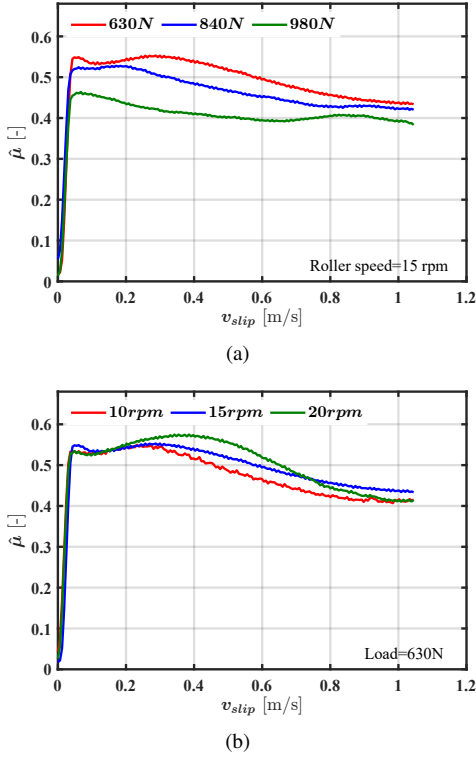


Fig. 12: Experimental results. Adhesion curve comparison at dry condition (a) Fixed roller speed, varying load; (b) Fixed load, varying roller speed.

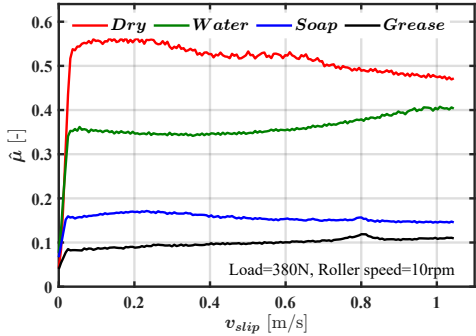


Fig. 13: Experimental results. Adhesion curve comparison for different conditions.

constant τ in (19). The LPF time constant of $\tau = 0.01$ s was chosen for all conducted experiments.

C. Anti-slip Control with Infinite Train Inertia

This test is performed to verify the direct method of anti-slip control (Section II-B) with fixed roller speed mentioned in Section IV-B. Wheel is in torque control mode ①, a torque ramp is provided (see top sub-figure in Fig. 14) along with slip control ② as shown in Fig. 4. The roller is in speed control and commanded a fixed speed. The equivalent force will get transferred from the wheel onto the roller until the adhesion reaches the maximum value (see bottom sub-figure in Fig. 14). Once the maximum adhesion is reached, the wheels begin to slip as shown in the second sub-figure in Fig. 14 and follows

the slip velocity command (see third sub-figure in Fig. 14). This is consistent with the discussion in subsection IV and the simulation results shown in Fig. 10.

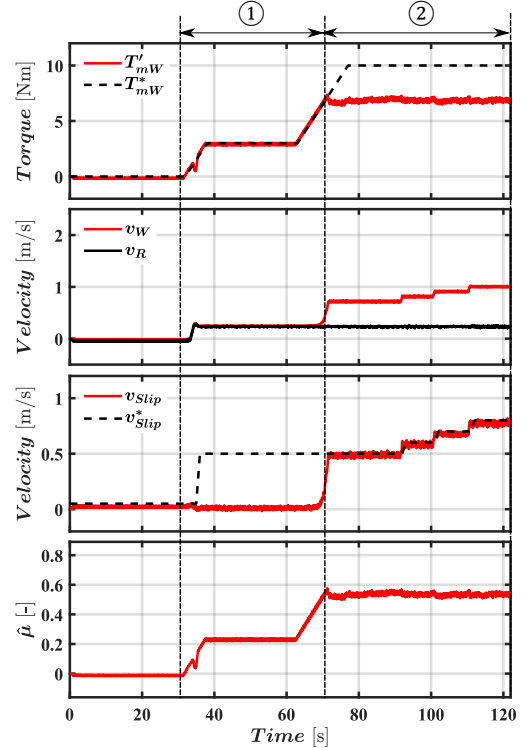
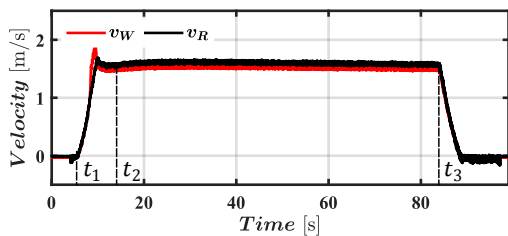


Fig. 14: Experimental results. Anti-slip control with fixed roller speed. From top to bottom: wheel torque; wheel and roller velocities; Commanded and actual slip velocities and estimated adhesion. ①: Torque control mode; ②: Slip control mode.

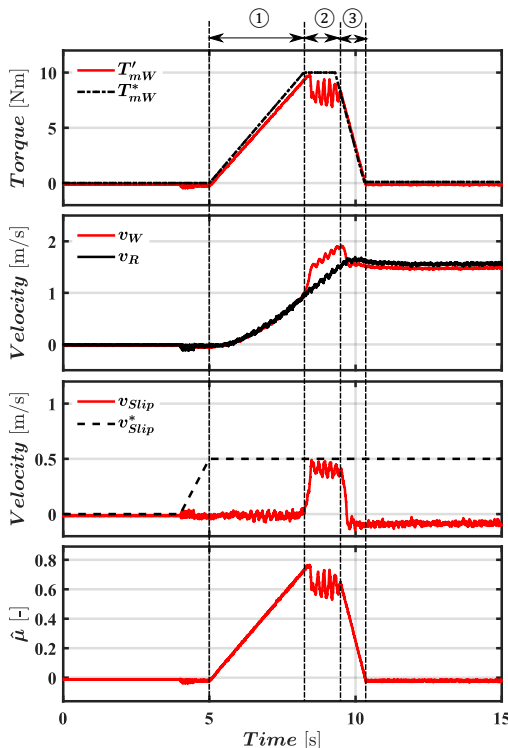
D. Anti-slip Control with Proposed Train Inertia Emulation using Disturbance Observer

The method explained in Section IV-C (Fig.8) is verified in the test bench. It includes the inertia emulation proposed in this paper. In this method both wheel and roller are in torque control. A ramp torque command (Fig. 15) is provided to the wheel. Once wheel starts rotating, roller starts rotating too. Inertia emulator block calculates the load torque required to emulate the train inertia, which is provided to roller drive.

Test results are shown in Fig. 15(a), the analysis being similar to the previous subsection. The ramp torque applied in Fig. 15(b) causes wheel and roller speed to increase slowly until maximum adhesion is reached. The wheel begins to slip and follows the slip command (see third sub-figure in Fig. 15(b)) after reaching the maximum adhesion value. It is observed that once the torque is removed, wheel and roller speeds remain almost constant, as would correspond to a system with a very large inertia. This effect becomes more evident in Fig. 15(a), where the system seems to maintain an almost constant speed for a large time span. This is in agreement with the simulation results shown in Fig. 10. Interestingly, it is observed from Fig. 15(a) that when the



(a)



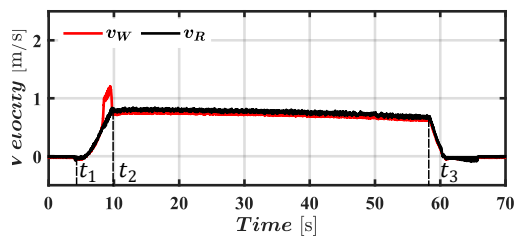
(b)

Fig. 15: Experimental results. Inertia emulator using Disturbance Observer method. (a) wheel and roller velocities. $t = t_1 \rightarrow t_2$, acceleration process; $t = t_2 \rightarrow t_3$, inertia emulation enabled; $t > t_3$, inertia emulation disabled. (b) Zoomed view of acceleration period showing from top to bottom: wheel torque; wheel and roller velocities; commanded and actual slip velocities and estimated adhesion. ① and ③: torque control mode; ②: slip control mode.

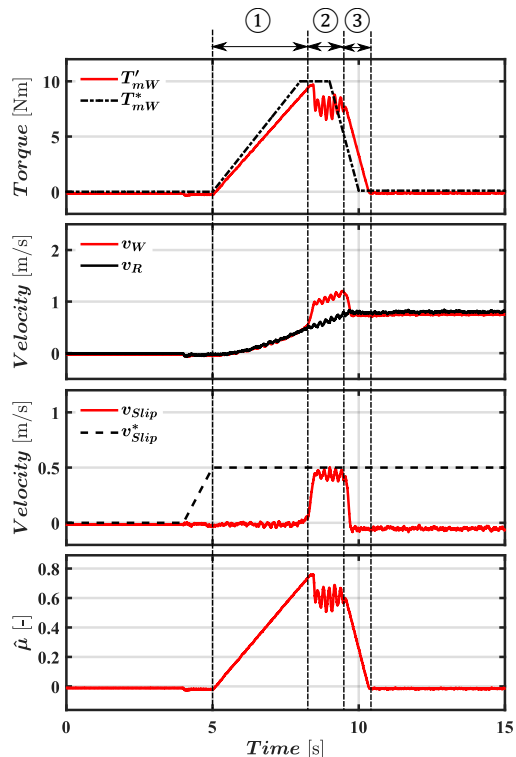
inertia emulation is disabled, wheel and the roller come to halt in a few seconds, due to the reduced inertia and relatively large friction of the physical system compared to the one being emulated.

E. Anti-slip Control with Proposed Train Inertia Emulation using Adhesion Torque Observer

The method proposed in this paper explained in Section IV-D (Fig.9) was also verified in the test bench. The test conditions and implementation methodology are the same as for the previous subsection. Test results are shown in Fig. 16, the analysis being similar as for the previous subsection too. The ramp torque applied in Fig. 16(b) causes wheel and roller



(a)



(b)

Fig. 16: Experimental results. Same legends as Fig. 15 using Adhesion Torque Observer method.

speed to increase slowly until maximum adhesion value is reached (see bottom sub-figure in Fig. 16(b)). The wheel begin to slip and follows the slip command (see third sub-figure in Fig. 16(b)) after reaching the maximum adhesion value. Once the torque command is reduced to zero, roller speed is seen to decrease slowly, but with a slope which is larger compared to the Disturbance Observer method shown in Fig. 15(a). This is in agreement with the simulation results shown in Fig. 10 where the slope of roller speed when the torque command is limited, is larger in Adhesion Torque Observer method compared to Disturbance Observer method for inertia emulation.

Finally, it is highlighted the importance of having a precise estimation of test bench friction \hat{B} in the 'Test bench dynamic model' of Fig. 9(a). This allows isolating the adhesion force in the estimation. Fig. 17(a) and Fig. 17(b) show the effects of underestimating and overestimating the friction respectively. Underestimation of friction results in a deceleration of $-0.019m/s^2$, which is around ten times faster than the

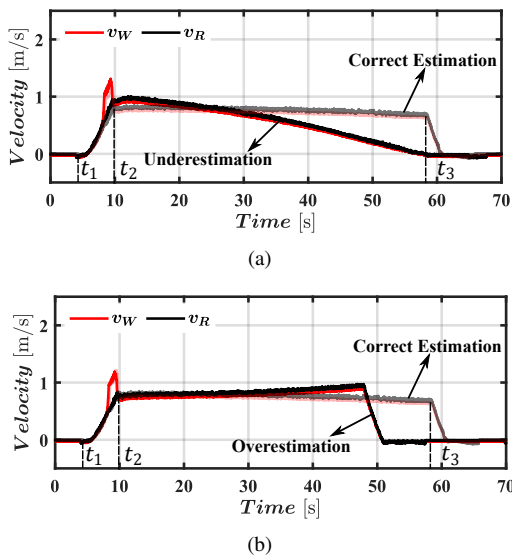


Fig. 17: Experimental results. Inertia emulator sensitivity to friction coefficient \hat{B} using Adhesion Torque Observer method. Wheel and roller velocities for the case of (a) underestimated and (b) overestimated \hat{B} .

expected value obtained using the actual train inertia and friction, which is $-2.08 \times 10^{-3} m/s^2$. Furthermore, in the case of overestimation of friction, the estimated train speed would not decrease but increase with an acceleration of $4.6 \times 10^{-3} m/s^2$. The importance of accurate test bench friction coefficient estimation becomes evident from these results.

VI. CONCLUSION

This paper explains the development of test bench intended for validation of anti-slip control for railway traction systems. System scaling and characterization of adhesion properties has been discussed in detail. The main contribution of the paper is the emulation of inertia, which is required for proper evaluation of anti-slip control. Two different approaches have been proposed. The first method uses a Disturbance Observer which emulates the train inertia irrespective of the test bench properties. The method with Adhesion Torque Observer produces torque command for the roller which reflects the desired properties of the train. This accounts for the traction force that gets transferred from wheel onto the roller including the inertia and friction of test bench. Thus the inertia emulation provides a good replica of the real train model. The concepts developed were first simulated and further verified experimentally in a roller-rig test. Train inertia emulation will require precise knowledge of roller-rig test bench inertia and friction. Roller-rig inertia can be estimated with good accuracy from the dimensions and material of the wheels. Friction estimation from system parameters is far more problematic, mainly due to the use of belts in the mechanical transmission. Therefore its adjustment has been performed experimentally. It has been shown that without proper adjustment of roller-rig parameters, inertia emulation is not reliable. Without proper inertia emulation, train acceleration and consequently the dynamic behavior of anti-slip control may be subjected to large deviations with

respect to read world behavior, eventually compromising the validation process.

REFERENCES

- [1] P. Pichlík, "Strategy of railway traction vehicles wheel slip control," *Czech Technical University, Prague*, 2018.
- [2] F. Trimpe and C. Salander, "Wheel-rail adhesion during torsional vibration of driven railway wheelsets," *Vehicle System Dynamics*, vol. 59, no. 5, pp. 785–799, 2021.
- [3] S. Iwnicki, *Handbook of railway vehicle dynamics*. CRC press, 2006.
- [4] A. Jaschinski, "On the application of similarity laws to a scaled railway bogie model." Ph.D. dissertation, Delft University of Technology, 1991.
- [5] R. Stock, D. T. Eadie, D. Elvidge, and K. Oldknow, "Influencing rolling contact fatigue through top of rail friction modifier application—a full scale wheel-rail test rig study," *Wear*, vol. 271, no. 1-2, pp. 134–142, 2011.
- [6] R. Conti, E. Meli, and A. Ridolfi, "A full-scale roller-rig for railway vehicles: multibody modelling and hardware in the loop architecture," *Multibody System Dynamics*, vol. 37, no. 1, pp. 69–93, 2016.
- [7] T. Ishrat, "Slip control for trains using induction motor drive," Ph.D. dissertation, Queensland University of Technology, 2020.
- [8] X. Fang, S. Lin, Z. Yang, F. Lin, H. Sun, and L. Hu, "Adhesion control strategy based on the wheel-rail adhesion state observation for high-speed trains," *Electronics*, vol. 7, no. 5, 2018.
- [9] S. Z. Meymand, M. J. Craft, and M. Ahmadian, "On the application of roller rigs for studying rail vehicle systems," in *Rail Transportation Division Conference*, vol. 56116. American Society of Mechanical Engineers, 2013, p. V001T01A015.
- [10] A. F. Abouzeid, J. M. Guerrero, I. Muniategui, A. Endemaño, D. Ortega, and F. Briz, "Torque dynamics enhancement of railway traction drives using scalar control," in *2021 IEEE International Electric Machines & Drives Conference (IEMDC)*. IEEE, 2021, pp. 1–6.
- [11] A. Fathy Abouzeid, J. M. Guerrero, A. Endemaño, I. Muniategui, D. Ortega, I. Larrazabal, and F. Briz, "Control strategies for induction motors in railway traction applications," *Energies*, vol. 13, no. 3, p. 700, 2020.
- [12] T. Mei, J. Yu, and D. Wilson, "A mechatronic approach for anti-slip control in railway traction," *IFAC Proceedings Volumes*, vol. 41, no. 2, pp. 8275–8280, 2008.
- [13] M. Fleischer, R. W. de Doncker, and D. Abel, "Traction control for railway vehicles," *Institut für Stromrichtertechnik und Elektrische Antriebe*, 2019.
- [14] S. Senini, F. Flinders, and W. Oghanna, "Dynamic simulation of wheel-rail interaction for locomotive traction studies," in *Proceedings of the 1993 IEEE/ASME Joint Railroad Conference*. IEEE, 1993, pp. 27–34.
- [15] K. Kondo, "Anti-slip control technologies for the railway vehicle traction," in *2012 IEEE Vehicle Power and Propulsion Conference*. IEEE, 2012, pp. 1306–1311.
- [16] P. Pichlík and J. Zdeněk, "Overview of slip control methods used in locomotives," *Transactions on Electrical Engineering*, vol. 3, no. 2, pp. 38–43, 2014.
- [17] A. Jaschinski, H. Chollet, S. Iwnicki, A. Wickens, and J. Würzen, "The application of roller rigs to railway vehicle dynamics," *Vehicle System Dynamics*, vol. 31, no. 5-6, pp. 345–392, 1999.
- [18] M. B. Marshall, R. Lewis, R. S. Dwyer-Joyce, U. Olofsson, and S. Björklund, "Experimental Characterization of Wheel-Rail Contact Patch Evolution," *Journal of Tribology*, vol. 128, no. 3, pp. 493–504, 03 2006. [Online]. Available: <https://doi.org/10.1115/1.2197523>
- [19] A. Rovira, A. Roda, M. Marshall, H. Brunskill, and R. Lewis, "Experimental and numerical modelling of wheel-rail contact and wear," *Wear*, vol. 271, no. 5-6, pp. 911–924, 2011.
- [20] S. H. Park, J. S. Kim, J. J. Choi, and H.-O. Yamazaki, "Modeling and control of adhesion force in railway rolling stocks," *IEEE Control Systems Magazine*, vol. 28, no. 5, pp. 44–58, 2008.
- [21] J. M. Guerrero, C. Lumberas, D. D. Reigosa, P. Garcia, and F. Briz, "Control and emulation of small wind turbines using torque estimators," *IEEE Transactions on industry applications*, vol. 53, no. 5, pp. 4863–4876, 2017.
- [22] TEXAS INSTRUMENTS, TMDSCNCD28335 controlCARD. [Online]. Available: <https://www.ti.com/tool/TMDSCNCD28335>
- [23] M. Fischer, F. Szekeley, M. Frea, and S. Jennek, "Impact of slip at low adhesion conditions caused by various contaminants," *EuroBrake 2019 - Rail Wheel Contact and Adhesion*, May, 2019.



Nihal Vishnu Vantagodi (M'00) received the B.E. in Electrical and Electronics Engineering in 2017 from PES Institute of Technology, India and Erasmus Mundus joint M.S. degree in Sustainable Transportation and Electrical Power Systems from Sapienza University of Rome, Italy; University of Nottingham, UK and University of Oviedo, Spain in 2021. He was associated with AEC research group of Department of Electrical, Computer and Systems Engineering, University of Oviedo from Jan 2021 till Feb 2022 where his research included ac drives and traction control. From Apr 2022, he is associated with eRC system GmbH working on electric propulsion system for eVtol.



Ahmed Fathy Abouzeid (M'19) received the B.S. and M.S. degrees in Electrical Engineering from Port Said University, Port Said, Egypt, in 2012 and 2017, respectively. He is currently pursuing his Ph.D. Degree at the Department of Electrical, Electronic and Computer Engineering, University of Oviedo, Gijón, Spain. From September 2021 to December 2021, he was a Visiting Researcher at Deutsche Bahn (DB) Systemtechnik GmbH, Minden, Germany. Since 2013, he joined the Department of Electrical Engineering, Port Said University, Egypt, as a Demonstrator. Currently, he is on leave with the same department as an Assistant Lecturer. His research interests include power converters and ac drives, electric traction, and renewable energy systems.



Juan M. Guerrero (S'00-A'01-M'04-SM'21) received the M.E. degree in industrial engineering and the Ph.D. Degree in Electrical and Electronic Engineering from the University of Oviedo, Gijón, Spain, in 1998 and 2003, respectively. Since 1999, he has occupied different teaching and research positions with the Department of Electrical, Computer and Systems Engineering, University of Oviedo, where he is currently a Full Professor. From February to October 2002, he was a Visiting Scholar at the University of Wisconsin, Madison. From June 2007 to December 2007, he was a Visiting Professor at the Tennessee Technological University, Cookeville. His research interests include control of electric drives and power converters, electric traction, and renewable energy generation. He is an Associate Editor of the IEEE TRANSACTIONS ON INDUSTRY APPLICATIONS.



Iban Vicente-Makazaga graduated in electrical engineering from University of Mondragon, Mondragon, Spain, in 2003 and the M.S. and the Ph.D. degrees from the University of Manchester, UK, in 2004 and 2009 respectively. He joined Ingeteam Power Technology (formerly TEAM), Zamudio, Spain, where he worked as a Control and Regulation Engineer involved in railway traction as an expert in power converter and advanced control drives, modulation and estimation techniques, AC catenary stability and mechanical vibrations in the drive-train. He joined Tecnalia, Derio, Spain, in 2022 where he works a senior researcher in automotive and aerospace projects. His current research interests include system engineering, V&V processes, high-integrity systems, functional safety standards and DevOps.



Iker Muniategui-Aspiazu received the Industrial Technical Engineering Degree (Electronic Design speciality) and the Industrial Automatics and Electronics Engineering Degree, from the University of Mondragon, Mondragon, Spain, in 2004 and 2007 respectively. In September 2006, he joined Ingeteam Power Technology (formerly TEAM), Zamudio, Spain, where he worked as a Control and Regulation Engineer, and he is currently Control and Regulation manager of Traction department. His current research interests include power converter and advanced control drives, modulation techniques, railway research issues such as AC catenary stability and mechanical vibrations in the drive-train.



Aitor Endemaño-Isasi received the Industrial Technical Engineering Degree (Electronic Design speciality) and the Industrial Automatics and Electronics Engineering Degree, from the University of Mondragon, Mondragon, Spain, in 1997 and 2000 respectively, and the PhD from Heriot-Watt University, Edinburgh, Scotland, UK, in 2003. In 2003 he joined Traction department at Ingeteam Power Technology (formerly TEAM), Zamudio, Spain, where since then he has been a Control and Regulation Engineer, involved in several traction control design projects for trams, locomotives and EMU-s. His current research interests include power converter and advanced control drives, modulation techniques, railway research issues such as AC catenary stability and mechanical vibrations in the drive-train.



Fernando Briz (A'96-M'99-SM'06) (Senior Member, IEEE) received the M.S. and Ph.D. degrees from the University of Oviedo, Gijón, Spain, in 1990 and 1996, respectively. He is currently a Full Professor with the Department of Electrical, Computer and Systems Engineering, University of Oviedo. His research interests include electronic power converters and ac drives, power systems, machine monitoring and diagnostics, and digital signal processing. Dr. Briz was the recipient of the IEEE TRANSACTIONS ON INDUSTRY APPLICATIONS Award and nine IEEE Industry Applications Society Conference and IEEE Energy Conversion Congress and Exposition prize paper awards. He is currently Chair of the Industrial Power Conversion System Department (IPCSD) of the IAS and Deputy Editor in Chief and member of the Steering Committee of IEEE JOURNAL OF EMERGING AND SELECTED TOPICS IN POWER ELECTRONICS (JESTPE). He is also member of the Executive Board of ECCE, and Past Chair of the Industrial Drives Committee of IPCSD. He has served in scientific committees and as Vice Chair or Technical Program Chair of several conferences, including ECCE, IEMDC, ICEM, ICEMS, and SLED and is an Associate Editor of IAS Transactions.